Spin structure and first-order transition of GdIn₃: Near-surface magnetism, buried amplitude-modulated phase, and interface delocalization

A. Malachias,[1] E. Granado,[2,1,][*] R. Lora-Serrano,[2] P. G. Pagliuso,[2] and C. A. Pérez[1]

[1]*Laboratório Nacional de Luz Síncrotron, Caixa Postal 6192, Campinas, CEP 13083-970, São Paulo, Brazil*
[2]*Instituto de Física "Gleb Wataghin," UNICAMP, Caixa Postal 6165, Campinas, CEP 13083-970, São Paulo, Brazil*

A resonant x-ray magnetic diffraction study was performed for pure and (Cd,Ga)-doped GdIn₃ single crystals with cubic structure. All studied samples show an equal-magnitude antiferromagnetic spin structure with propagation vector $\vec{\tau}=[\frac{1}{2},\frac{1}{2},0]$ at low temperatures, corresponding to a parallel spin propagation along the $\vec{c}$ direction (normal to the studied surfaces) and antiparallel propagation along $\vec{a}$ and $\vec{b}$. A complex magnetic behavior in the submicrometric near-surface region (NSR) was found close to $T_N^{bulk} \sim 44$ K. For both pure and substituted samples, a fairly strong signal from the equal-magnitude magnetic phase was found to survive above T_N^{bulk} and abruptly disappears at $T_N^{NSR} \sim T_N^{bulk}+0.7$ K, indicating that the NSR may show a larger T_N than the bulk for all studied samples. For the pure compound only, satellite peaks consistent with an amplitude-modulated magnetic phase with a wavelength of 380 Å were found between T_N^{bulk} and T_N^{NSR}. A successful fit of the scattering profile around several magnetic Bragg positions and photon energies, using a simple phase coexistence model, confirmed that the amplitude-modulated phase develops underneath the most superficial region showing the equal magnitude structure. The evolution of the magnetic scattering profile on cooling indicates that the interface between equal-magnitude and amplitude-modulated phases diverges towards the bulk as $T \to T_N^{bulk}$ from above. A detailed analysis of the magnetic scattering, as well as the existence of a single bulk transition within the experimental sensitivity of our specific heat and magnetic susceptibility measurements, in contrast to the rich behavior shown by the near-surface region, indicates that the amplitude-modulated phase is not bulk representative, being actually sandwiched between the bulk paramagnetic and the equal-magnitude phases. Depth-temperature phase diagrams for pure and (Ga,Cd)-doped GdIn₃ are drawn on the basis of our results, which are discussed in terms of a three-phase coexistence scenario theoretically proposed for first-order transitions in the NSR.

I. INTRODUCTION

It is well known that the near-surface region (NSR) in condensed matter may show a distinct behavior with respect to the bulk at the vicinity of a phase transition (for reviews on this subject, see Refs. 1–4). In some cases, the relevant interaction at the surface may be enhanced, leading to a larger transition temperature in the NSR than in the bulk ($T_c^{NSR} > T_c^{bulk}$). The bulk ordering transition at T_c^{bulk} is then termed "extraordinary," as opposed to the "ordinary" transition for which $T_c^{NSR} = T_c^{bulk}$. The behavior of the NSR in first-order transitions have been first dealt theoretically by Lipowsky and co-workers,[5,6] and the interface between the bulk and NSR phases was predicted to become delocalized. Thus, for extraordinary transitions, the ordered phase would be nucleated in the surface at T_c^{NSR}, propagating toward the bulk as T decreases and approaches T_c^{bulk}.[6] An interesting and somewhat counterintuitive consequence of such theory is the possibility of a NSR with macroscopic thickness for temperatures sufficiently close to T_c^{bulk}. Thus, in a limited temperature interval, the very existence of a surface may in principle disturb the physical state of a system at much larger depths than the typical interaction range that ultimately drives the transition. Direct observations of the interface delocalization in the nanometric scale have already been reported. For instance, Frenken and van der Veen[7] were able to observe the melting of the Pb(110) surface by ion-scattering experiments, with an increase in the thickness of the liquid surface film as T approaches the melting temperature. Also, Dosch et al.[8] investigated the bulk order-disorder transition in a Cu₃Au(100) surface by means of grazing-incidence x-ray diffraction and also attested a divergence of the surface layer thickness at the transition.

In magnetic systems, the experimental investigations on extraordinary phase transitions were performed mostly in the context of the so-called "second length scale." In a variety of compounds, anomalously sharp diffraction profiles in the vicinity of magnetic phase transitions have been observed and attributed to the presence of near surface-induced antiferromagnetism.[9–15] To our knowledge, the most detailed investigations on near-surface magnetism have been done by resonant x-ray diffraction experiments on uranium compounds such as uranium phospide[16] or uranium dioxide,[17] in which advantage of the very strong resonance of the U M_{IV} edge was taken to reveal in detail the depth-dependent ordered magnetic moments. The results for UP clearly indicate the formation of extended sheets of ferromagnetically aligned moments parallel to the sample surface. These sheets are antiferromagnetically coupled in the direction normal to the surface, a few layers deep, above the bulk antiferromagnetic (AFM) ordering temperature.[16] This near surface magnetism disappears at a given temperature slightly above the bulk transition temperature. More recently, nonresonant magnetic x-ray diffraction experiments were performed in NiO in grazing-incidence geometry with controlled penetration depths,[15] also showing distinct behavior of the surface with

respect to the bulk within a scale of the order of a few nanometers. In this context, we should also mention a very direct observation of magnetic interface delocalization in the AFM transition of $FeBO_3$ by means of depth-selective Mössbauer measurements in a near-surface magnetic phase being observed in a length scale between 1 and 500 nm, depending on the proximity to T_N^{bulk}.[18]

All the experimental reports described above investigate a phase transition between an ordered and a disordered state, i.e., either solid-liquid or AFM-paramagnetic transitions. So far unexplored, to our knowledge, is the near-surface behavior in systems in which two distinct ordered phases, or even two ordered and a third disordered phase, compete through first-order transitions. It is clear that more experimental work in interface delocalization and related phenomena at first-order transitions is necessary to test theoretical predictions and, perhaps, reveal new unexplored physics, giving strong motivation for near-surface investigations in many classes of compounds. A potentially interesting class may be superconductors at the verge of magnetism, where the near-surface region may have a different behavior than the bulk. For instance, the heavy-fermion $CeIrIn_5$ shows distinct bulk and surface superconducting temperatures,[19] which remain unexplained. In fact, the compound studied in this work, $GdIn_3$, is a counterpart of $CeIn_3$ which is the parent cubic compound of the tetragonal $CeIrIn_5$ and other structurally related heavy fermion superconductors in the same family.[19,20] Rare-earth-based magnetic materials in this family have also been studied to understand in detail the evolution of the $4f$ magnetism in this series and its role in the occurrence of heavy fermion superconductivity in the Ce-based systems.[21,22]

In this paper, we report a resonant x-ray diffraction investigation of the magnetic structure critical behavior of pure and (Cd, Ga)-doped $GdIn_3$, complemented by specific heat and dc-magnetic susceptibility measurements. Our results show a complex depth-dependent magnetic profile in the submicrometric scale, where three distinct magnetic phases—equal-magnitude AFM (EM-AFM), amplitude-modulated AFM (AM-AFM), and paramagnetic (PM)—seem to coexist in an organized manner close to the surface of single crystals of pure $GdIn_3$. The dilute substitutions of Ga and Cd in the In site are shown to have a deep impact in the delicately balanced three-phase coexistence found in the pure compound. Our results are interpreted as manifestations in the submicrometric scale of interface-delocalization phenomena in extraordinary phase transitions,[5,6] with additional physics arising from a competition between two distinct ordered states close to T_N.[23]

II. EXPERIMENTAL DETAILS

Four batches of single crystalline $GdIn_3$:(Cd,Ga) samples (two pure and one for each substitution) with sizes up to 4 mm³ were grown from an In flux,[20] mixed with Cd or Ga flux when applicable. The Cd/In and Ga/In proportions for the doped samples were obtained by x-ray fluorescence analysis using the XRF beamline of the Laboratório Nacional de Luz Síncrotron (LNLS). The quantitative analysis was performed with the WINAXIL software[24] based on the funda-

TABLE I. Composition, Néel temperature, and room-temperature lattice parameters for the compounds investigated in this work.

Sample	Composition	T_N^{bulk} (K)	a (Å)
GdIn₃	$GdIn_3$	44.15	4.6066(4)
GdIn₃:Cd	$GdIn_{2.937(5)}Cd_{0.063(5)}$	43.8	4.6085(8)
GdIn₃:Ga	$GdIn_{2.941(1)}Ga_{0.059(1)}$	44.8	4.5997(8)

mental parameter method.[25] In order to correctly discriminate the overlapping effect between the Cd and In fluorescence L lines for the particular case of $GdIn_3$:Cd sample, the intensity ratios between L lines of the same element were kept fixed in the fit using the tabulated values.[26] Assuming that pure $GdIn_3$ samples were stoichiometric and could be used as a calibration standard, it was found that $R=[n(In)+n(Ga)]/n(Gd)$ or $R=[n(In)+n(Cd)]/n(Gd)$ were also close to the stoichiometric values of 3.00 for the doped samples, within ~2%. This indicates that there is no significant level of atomic vacancies within the structure of these samples. We subsequently fixed $R=3.00$ and obtained the relative Cd(Ga)/In concentration from the relative intensity of the respective fluorescence lines. The so obtained compositions, together with the lattice parameters of the studied samples at room temperature, are shown in Table I.

Specific heat measurements were performed in a commercial physical property measurements system platform using the relaxation method. dc magnetic susceptibility measurements were taken with a superconducting quantum interference device magnetometer.

Selected crystals with naturally formed (001) surfaces were finely polished in alumina powder (0.05 μm) for several hours, yielding mosaic widths of $\leq 0.1°$ full width at half maximum (FWHM) and sealed in Ar atmosphere. X-ray diffraction measurements were performed at the XRD2 bending magnet beamline of LNLS.[27] A commercial closed-cycle He cryostat was mounted into the Eulerian cradle of a 4+2 circle diffractometer, and the sample was kept under low vacuum ($<10^{-3}$ mbar) during measurements. The thermal accuracy and stability were better than ~0.5 and ~0.05 K, respectively. The sample was mounted with (00l) reflections being in specular condition, while the scattering plane accessible without sample tilts was (0kl). (hkl) planes with $h \neq 0$ were then accessed by tilting the sample through the Euler circle. The measurements were made in coplanar geometry with linearly σ-polarized incident photons in dipolar resonance conditions at the Gd L_{II} edge (7.932 keV) except where otherwise stated, with an energy resolution of ~5 eV. The beam dimensions at the sample position were 0.6 mm (V) $\times 2.0$ mm (H). Crystal truncation rod measurements along the [00l] direction were performed to probe the surface roughness of a pure $GdIn_3$ sample after polishing. l scans spanning from $l=1.1$ to $l=6.4$ were measured at 10 keV. Following the procedure established by Robinson[28] a root-mean-square roughness of 7.8(5) Å and a lateral roughness length scale of 2700(50) Å were obtained, indicating a very good surface quality.
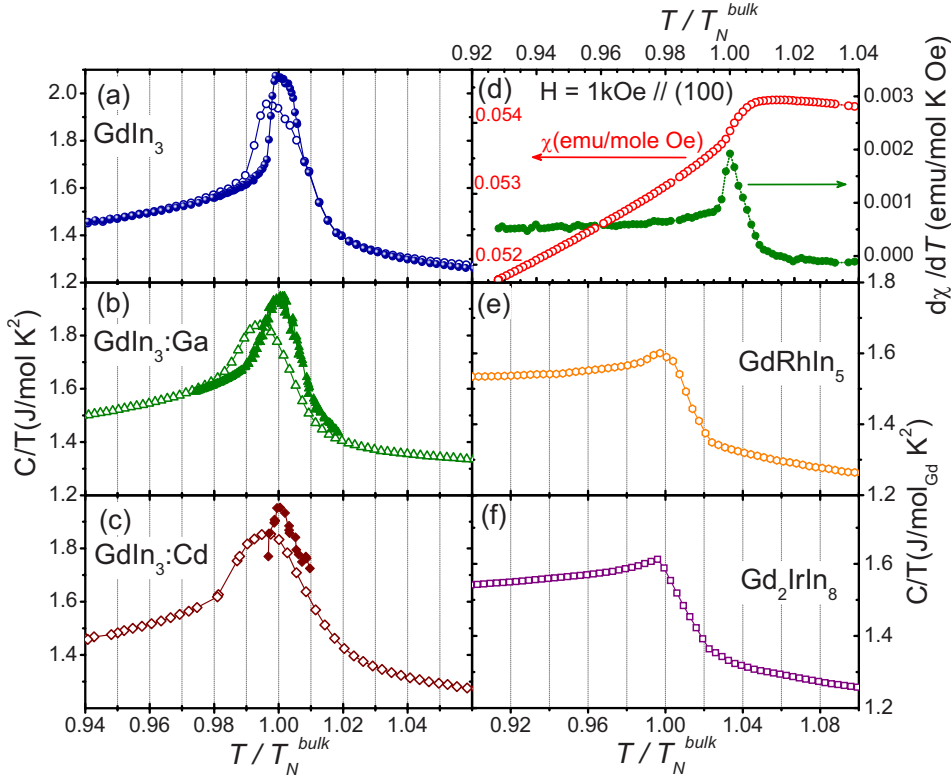
FIG. 1. (Color online) Specific heat of (a) GdIn$_3$, (b) GdIn$_3$:Ga, (c) GdIn$_3$:Cd, (e) GdRhIn$_5$, and (f) Gd$_2$IrIn$_8$, close to the bulk AFM-paramagnetic transition temperature. (d) dc-magnetic susceptibility $[\chi_{dc}(T)]$ and its temperature derivative for GdIn$_3$ for an applied field of 1000 Oe along the [100] direction.

III. RESULTS AND ANALYSIS

A. Specific heat and dc-magnetic susceptibility

Specific heat (C_p) measurements are given in Figs. 1(a)–1(c) for pure GdIn$_3$, as well as for the Ga- and Cd-doped samples, respectively. Two sets of measurements were performed using the relaxation method. First, a condition with a broader resolution in temperature but higher sensitivity was employed, setting the relaxation temperature sweep at 0.1 K at each step (open symbols). In the second set of measurements, this parameter was reduced to 0.02 K, only in a limited temperature region around the transition (filled symbols). No further changes were observed using even smaller relaxation temperature sweeps. It can be seen that both pure and (Ga,Cd)-doped GdIn$_3$ exhibits a clear peaklike feature at T_N. This is indicative of a single bulk phase transition for GdIn$_3$ in the studied temperature interval, with a weakly first-order character. For the sake of comparison, C_p measurements for the related GdRhIn$_5$ and Gd$_2$IrIn$_8$ compounds are given in Figs. 1(e) and 1(f), respectively, with steplike features at T_N indicative of second-order phase transitions, which is consistent with previous magnetic x-ray diffraction studies.[29,30]

dc-magnetic susceptibility measurements, $\chi_{dc}(T)$, were taken for pure GdIn$_3$ in both sweep and no overshoot modes at the vicinity of T_N, with a cooling rate of 0.05 K/min with applied fields of 100 and 1000 Oe along both the [100] and [110] directions. A representative measurement, taken with 1000 Oe along the [100] direction, is shown in Fig. 1(d). Again, a single bulk magnetic transition was seen within our resolution, in contrast to similar investigations showing multiple bulk transitions at the vicinity of T_N in other members

of the RIn$_3$ family (R=rare earth).[31] These measurements reinforce the conclusion of a single *bulk* phase transition for GdIn$_3$ at the vicinity of T_N. The transition temperatures obtained for each sample are given in Table I.

B. Resonant magnetic x-ray diffraction

1. Magnetic state at low temperatures

We start the description of our x-ray diffraction results by solving the magnetic structure of GdIn$_3$ at low temperatures. At $T \gg 45$ K, only charge scattering is observed in positions consistent with the symmetry of this material (space group $Pm3m$). At 12 K, additional reflections were found at ($i + \frac{1}{2}, j + \frac{1}{2}, l$) ($i$, j, and l integers) reciprocal space positions. The energy dependence of the intensity of the ($\frac{1}{2}, \frac{3}{2}, 3$) Bragg peak for the pure sample through the Gd L_2 and L_3 edges is given in Fig. 2. The absorption coefficient of the sample, obtained from the fluorescence yield taken in the θ-2θ geometry, after applying corrections from self-absorption effects, is also shown in Fig. 2, within an estimated accuracy better than ~5% at the resonances. Clear resonances in the Bragg peak can be seen, with maxima located ~2 eV above the absorption edges defined at the energies of maximum inflection of the absorption coefficient. Typical count rates of a few thousand counts/s were obtained for the strongest magnetic reflections in resonant conditions at low temperatures. A polarization analysis of the signal at the L_2-edge resonance was also performed, confirming pure σ-π scattering. The resonance and polarization properties of this signal, as described above, clearly indicate that these additional reflections are magnetic and arise from dipolar resonances. The
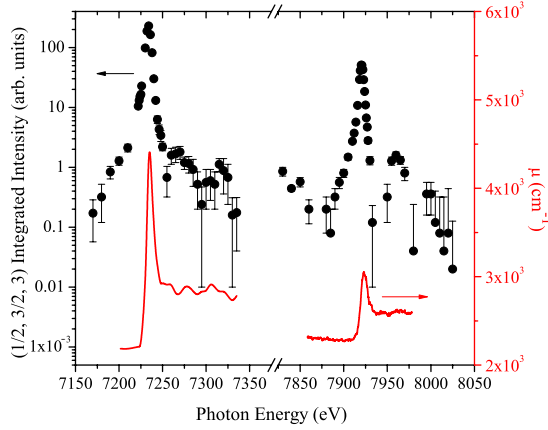
FIG. 2. (Color online) Energy dependence of the magnetic intensity of the $(\frac{1}{2}, \frac{3}{2}, 3)$ Bragg peak around the Gd L_2 and L_3 edges. The absorption coefficient obtained from the fluorescence yield are indicated with solid lines.

reciprocal space positions of such magnetic Bragg peaks then indicate a commensurate Gd spin structure with propagation vector $\vec{\tau} = [\frac{1}{2}, \frac{1}{2}, 0]$.

The moment direction can be obtained from the intensities of a set of magnetic reflections. In fact, for collinear magnetic structures and σ-polarized incident photons, the polarization dependence of the x-ray magnetic scattering assumes a simple form for dipolar resonances,[32,33] and the intensities of magnetic Bragg peaks are given by $I^M(\vec{\tau}) \propto [\Sigma_j \vec{m}_j \cdot \vec{k}_f \cos(\vec{\tau} \cdot \vec{r}_j)]^2$, where the sum is over the *j*th resonant ion in the magnetic unit cell, $\vec{r}_j$ is the position of such an ion, $\vec{\tau}$ is the reciprocal lattice vector for the Bragg reflection, $\vec{m}_j$ is the magnetic moment at site *j*, and $\vec{k}_f$ is the wave vector of the scattered light. This expression is valid as long as the quadratic term in $\vec{m}_j$ on the magnetic scattering amplitude can be neglected.[32,33] The magnetic structure was thus resolved by comparing the intensities of the accessible magnetic Bragg reflections with those expected assuming distinct physical models with collinear Gd magnetic moments using the expression given above for $I^M(\vec{\tau})$. These reflections were measured at 12 K using a beam size of 0.2 (V) × 1.0 (H) mm², limited by slits, which warranted that the entire beam hit the sample surface for all studied reflections. For the nonspecular magnetic Bragg peaks studied here, an (h,k,l)-dependent absorption factor must be taken into account. Thus, the measured intensities were divided by a correction term given by $\sin(\beta)/[\sin(\beta) + \sin(\gamma)]$, where β and γ are the angles between the surface and the diffracted and incident beam directions, respectively. The results are given in Table II for a pure GdIn₃ sample. It was unambiguously found that the magnetic moments point toward the $\vec{c}$ direction, i.e., in the direction of the ferromagnetic chains and along to the normal to the sample surface. Similar analyses performed in a second pure GdIn₃ sample, as well as in the Cd- and Ga-doped samples yield the same conclusion. Figure 3 displays the low-*T* EM-AFM structure of GdIn₃.

It is interesting to mention that magnetic reflections related to the symmetry-equivalent $\vec{\tau} = [\frac{1}{2}, 0, \frac{1}{2}]$ and $\vec{\tau} = [0, \frac{1}{2}, \frac{1}{2}]$ were not observed in any of the studied samples, at

TABLE II. Comparison between observed and calculated intensities of magnetic Bragg reflections at 12 K, normalized by the most intense reflection, assuming the moments $\vec{m}$ along each one of the three axis of the unit cell. The particular choice of cubic axes was made so that the $\vec{c}$ axis is the surface normal, while the scattering plane without sample tilts is $(0kl)$. Experimental data were taken on resonance conditions, 2 eV above the Gd L_{II} edge.

(h,k,l)	I_{obs}	$\vec{m} \parallel \vec{a}$	$\vec{m} \parallel \vec{b}$	$\vec{m} \parallel \vec{c}$
$(-\frac{1}{2}, -\frac{1}{2}, 2)$	2	1	100	2
$(-\frac{1}{2}, \frac{1}{2}, 3)$	51	12	58	50
$(-\frac{1}{2}, -\frac{1}{2}, 3)$	21	4	87	17
$(\frac{1}{2}, \frac{1}{2}, 3)$	52	12	58	50
$(\frac{1}{2}, -\frac{1}{2}, 3)$	19	4	87	17
$(\frac{3}{2}, \frac{1}{2}, 3)$	38	100	53	46
$(-\frac{3}{2}, \frac{1}{2}, 3)$	41	100	53	46
$(-\frac{1}{2}, \frac{1}{2}, 4)$	79	10	41	70
$(-\frac{1}{2}, \frac{3}{2}, 4)$	100	14	15	100

least in the near-surface region accessible to the x rays. This indicates that the ferromagnetic chains point always along the $\vec{c}$ direction (defined here as the normal to the polished surface), at least within the skin depth probed by the x rays (~1 μm). This unexpected absence of AFM domains in the NSR appears to be a surface-induced effect and will be further discussed in Sec. IV.

2. Inhomogeneous magnetic state at $T \sim T_N$

The equal magnitude phase resolved above was found to remain stable between the lowest studied temperature (12 K) and $T_N^{bulk} = 44.15$ K. For $T \gtrsim T_N^{bulk}$, broadened magnetic Bragg peaks were observed for all studied samples at nearly the same Bragg positions as for $T < T_N^{bulk}$. In addition, satellite magnetic peaks are clearly observed between T_N^{bulk} and T_N^{AM} ~ 44.6 K for the pure GdIn₃ samples, indicating that a new incommensurate magnetic phase develops in this temperature interval. Figure 4 shows two-dimensional *hl* maps in the vicinity of the $(\frac{3}{2}, \frac{1}{2}, 4)$ reciprocal space position at 39.4 K ($T \ll T_N^{bulk}$) and 44.4 K ($T_N^{bulk} < T < T_N^{AM}$), indicating that this discommensuration is associated with a magnetic structure with a propagation vector $\tau_2 = [\frac{1}{2}, \frac{1}{2}, \delta]$, with $\delta \sim 0.012$. Such
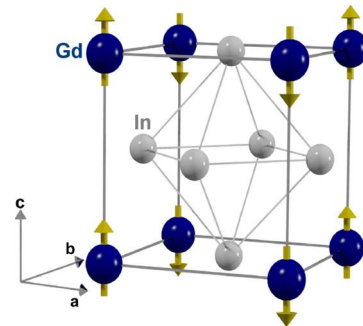

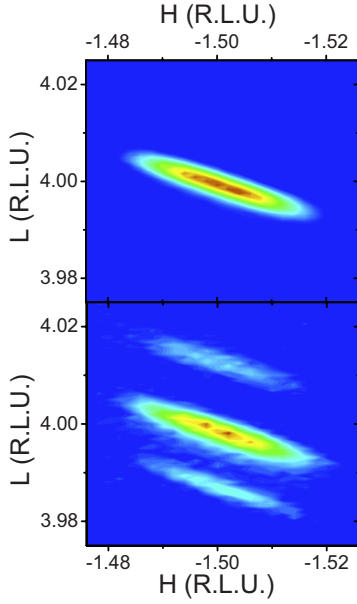FIG. 3. (Color online) Equal magnitude magnetic structure of GdIn₃ at 12 K.

FIG. 4. (Color online) hl reciprocal-space maps at the vicinity of the $(\frac{3}{2}, \frac{1}{2}, 4)$ magnetic Bragg reflection at 39.4 K (upper panel) and 44.4 K (lower panel). The shape of the scattering at 39.4 K is solely determined by the instrumental resolution convoluted with the sample mosaic width.

τ_2 corresponds to a long-wavelength variation of the magnetic scattering factor along the $\vec{c}$ direction, with a period of ~ 83 lattice parameters or ~ 380 Å. Additional kl and hk maps were also taken (not shown), corroborating this conclusion. Notice that due to the relatively large rocking widths of our samples ($\sim 0.1°$ FWHM), the resolution of a Bragg peak in reciprocal space is highly anisotropic in the form of an oblate ellipsoid oriented along the direction of the axial (θ-2θ) scans such as seen in Figs. 4(a) and 4(b).

The simultaneous observation of central and satellite peaks above T_N^{bulk} [see Fig. 4(b)] is not consistent with a simple homogeneous incommensurate magnetic phase. To understand this, we first note that a slight shift of the central peak at 44.4 K is observed toward lower l direction with respect to the integer values related to the bulk lattice parameters, while the satellite peaks remain symmetric with respect to the integer-l position within our resolution [see Figs. 4(b) and 5(a)–5(j)]. Similar asymmetric shifts close to T_N have been observed before in other compounds and attributed to effects arising from a finite correlation length.[34] The fact that the central and satellite peaks show distinct asymmetric shifts at a given temperature is a clear indication of distinct correlation lengths associated with each contribution. This suggests that central and satellite peaks arise from different domains of the sample, i.e., they result from a magnetically inhomogeneous state at this temperature.

To obtain further insight into the interesting state for $T \gtrsim T_N^{bulk}$ with two distinct types of magnetic order or correlations, the magnetic scattering at several magnetic Bragg planes was investigated. The x-ray penetration depth for each reflection can be calculated by the trivial relation $z = [\mu/\sin(\gamma) + \mu/\sin(\beta)]^{-1}$, where μ is the absorption coefficient of the material given in Fig. 2. Figures 5(a)–5(j) show
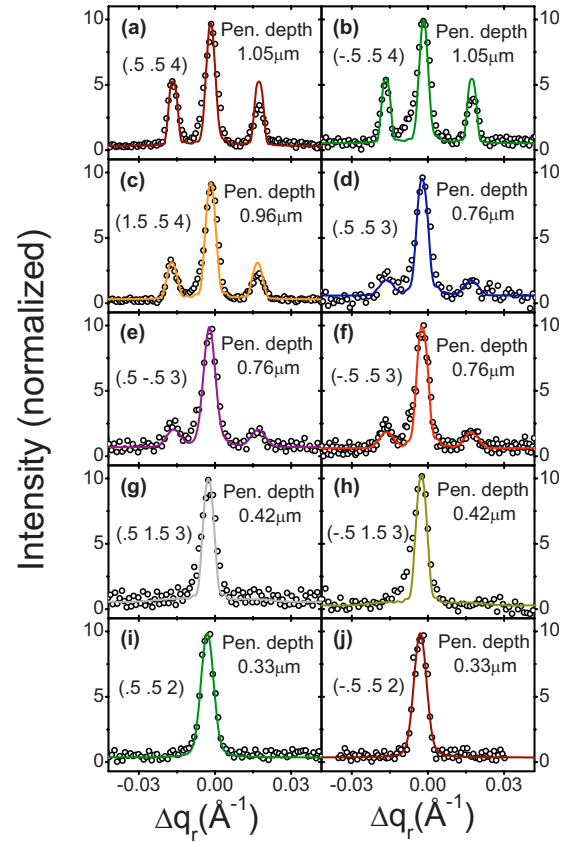

FIG. 5. (Color online) Measured (symbols) and simulated (lines) longitudinal scans at 44.4 K around the (a) $(\frac{1}{2}, \frac{1}{2}, 4)$, (b) $(-\frac{1}{2}, \frac{1}{2}, 4)$, (c) $(\frac{3}{2}, \frac{1}{2}, 4)$, (d) $(\frac{1}{2}, \frac{1}{2}, 3)$, (e) $(\frac{1}{2}, -\frac{1}{2}, 3)$, (f) $(-\frac{1}{2}, \frac{1}{2}, 3)$, (g) $(\frac{1}{2}, \frac{3}{2}, 3)$, (h) $(-\frac{1}{2}, \frac{3}{2}, 3)$, (i) $(\frac{1}{2}, \frac{1}{2}, 2)$, and (j) $(-\frac{1}{2}, \frac{1}{2}, 2)$ positions. Note the slight off-centering of the central peak with respect to the satellite peaks in (a)–(f).

the one-dimensional longitudinal (θ-2θ) scans at 44.4 K around ten reflections studied at this temperature (symbols). It is evident that a smaller (larger) penetration depth is associated with a more (less) intense central peak with respect to the satellite peaks. For the lowest penetration depths, shown in Figs. 5(g)–5(j), no satellites are observed within the sensitivity of our experiment. This is an indication that the central peak is associated with a NSR above T_N^{bulk}, while the satellite peaks arise from the region underneath this NSR. Notice that although our experimental setup did not allow for controlled penetration depths for each reflection, such as in Ref. 15, depth-selective information in the submicrometric scale could still be obtained in our experiment by probing several distinct magnetic Bragg reflections.

Figure 6(a) shows the energy dependence of the intensities of the central and sum of satellite peaks at the vicinity of the $(\frac{3}{2}, \frac{1}{2}, 4)$ Bragg position close to the L_2 edge at $T = 44.4$ K. The ratio between the satellite and central intensities is given in Fig. 6(b). It can be seen that this ratio is smallest at the vicinity of the absorption edge. This is an additional evidence that an AM-AFM phase develops underneath the NSR. In fact, at energies very close to an absorption edge, the penetration depth of the x rays is minimum
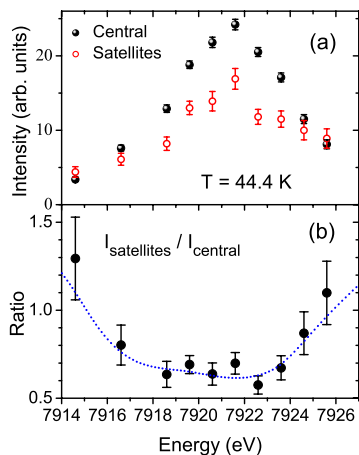
FIG. 6. (Color online) Energy dependence of (a) the intensity of the central and satellite peaks at the vicinity of the $(\frac{3}{2},\frac{1}{2},4)$ Bragg position at 44.4 K and (b) the ratio between the intensities of the satellite and central peaks. The dashed line in (b) is the prediction of our phase-coexistence model using the same parameters obtained in the fits of Figs. 5(a)–5(j) and the absorption coefficients of Fig. 2.

and the attenuation of the satellite peaks arising from the buried AM-AFM is larger than the corresponding effect from the central peak arising from the most superficial layer.

3. Kinematical model

To obtain quantitative information about the inhomogeneous magnetic state proposed above for $T \gtrsim T_N^{bulk}$, we performed a kinematical analysis of the overall magnetic scattering. According to our simple fitting model, a NSR with the EM-AFM structure displayed in Fig. 3 interfaces a second ordered layer with the AM-AFM structure, which in turn interfaces the bulk paramagnetic phase. This depth dependence of the sublattice magnetization is represented in Fig. 7(a). The free parameters in the model that affect the scattering intensities are (i) the order parameter amplitude m_0, represented by an overall scale factor in the intensities, and the thicknesses of the (ii) EM-AFM and (iii) AM-AFM phases, which impact both the peak widths and the relative intensities among the central and satellite peaks for each (h,k,l). Despite the apparent boldness of the model and the small number of free parameters, the resulting simulated x-ray diffraction profiles were successfully tested against all observed reflections with different penetration depths at $T=44.4$ K using the same set of parameters. The fits performed for each reflection are represented by the solid lines in Figs. 5(a)–5(j). The so obtained thicknesses at this temperature were 0.41(5) and 0.51(7) μm for the EM-AFM and AM-AFM phases, respectively. As an additional verification of our model, the ratio between the satellite and central intensities as a function of energy was predicted using the phase thicknesses obtained above and the absorption coefficients $\mu(E)$ given in Fig. 2. The results are given as a dashed line in Fig. 6(b) and agree well with the experimental data. The fact that this agreement was obtained without any free fitting parameter strongly argues in favor of our model.
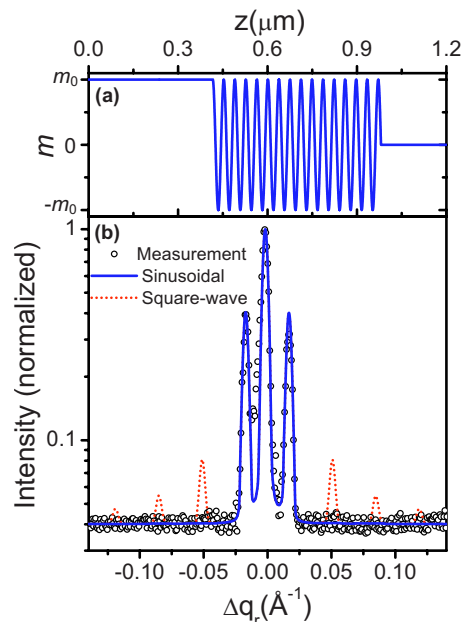

FIG. 7. (Color online) (a) Representation of the sublattice magnetization amplitude at 44.4 K, including a near-surface equal magnitude phase coexisting with a sinusoidal amplitude-modulated buried phase and a paramagnetic bulk phase. (b) Measured l scan at the vicinity of the $(\frac{3}{2},\frac{1}{2},4)$ magnetic reflection (dots) at 44.4 K. The solid line is obtained from the simulation of the magnetic profile shown in (a). The dashed line was obtained by the simulation of the equivalent profile with a buried square-wave AM-AFM layer, exhibiting additional higher order satellites that were not observed in our measurements.

It is valid to investigate in more detail whether the amplitude-modulated layer corresponds to a true sine-modulated phase or if it shows some squaring up (see, for example, Ref. 35). Figure 7(b) shows an l scan performed at the vicinity of the $(\frac{3}{2},\frac{1}{2},4)$ magnetic reflection at 44.4 K, taken with particularly long counting times, leading to a fairly good signal-to-noise ratio. The solid line represents the fit to the model described above, while the dashed lines represent the additional higher-order satellites expected for a square-wave intensity modulation. Clearly, our sensitivity is enough to rule out this latter possibility, and the absence of any observable higher-order satellite indicates that the amplitude modulation is described by a sine wave at this temperature in a good approximation.

Alternative models for the incommensurate phase were also considered. Particularly, an EM helical magnetic structure in the ab plane propagating along $\vec{c}$ also predicts the satellite peaks. However, since the intensities depend critically on the moment directions (see above), the calculated (h,k,l) dependence of the satellite peak intensities under the helical model shows large discrepancies with the relative peak and/or satellites intensity ratio obtained from the experiment (not shown). We mention that, to our knowledge, no compound with a single Gd ion in the crystallographic basis has been reported to show noncolinear EM order, which is indeed in agreement with the predictions of classical dipole-dipole exchange.[36] Of course, other possibilities

that account to the presence of the central and satellite peaks might still be envisaged. However, the uniqueness of our model with respect to entirely different solutions is supported by the number of reflections to which the scattering profiles were quantitatively tested [ten total and five independent reflections, see Figs. 5(a)–5(j)] in comparison to the number of free fitting parameters that affect the widths and relative intensities of central and satellite peaks (two, see above). Also, the energy-dependent data shown in Fig. 6(b) may be taken as an independent verification of the model. An analogy may be drawn to conventional crystallography, in which the solution of a given crystal structure is considered correct and unique if it successfully accounts for the intensities of a number of Bragg peaks that is larger than the number of free structural parameters. On the other hand, more elaborated scenarios that are similar to ours but in addition allows for a smoother depth dependence of the magnetic order parameter within each phase and at the interfaces, therefore requiring a larger number of fitting parameters, are not discarded (see, for example, Ref. 37). Here, we consider each phase (EM-AFM, AM-AFM, and PM) as internally homogeneous, leading to a picture with a minimal number of fitting parameters while still being able to capture the essential physics revealed by our data. A more detailed analysis of the sublattice magnetization profile within each phase requires a more complete set of experimental data, possibly using a grazing-incidence diffraction geometry such as in Ref. 15, and is beyond the scope of the present work.

The only experimental aspect not satisfactorily captured by our model is the asymmetry between the left and right satellite intensities [see Figs. 5(a)–5(f)]. An investigation of a second GdIn$_3$ pure sample showed that the sign of this asymmetry is sample dependent, indicating an extrinsic origin. The miscut of the crystal surface with respect to the bulk lattice that results from the polishing process is one possible source of asymmetry in this system. Such small miscut is essentially random in our sample preparation process.

4. Temperature dependence

Having evidenced the essential correctness of our simulation model at a fixed temperature, we have performed an investigation of the depth and temperature dependences of the magnetic structure of GdIn$_3$. Figures 8(a)–8(h) show longitudinal (θ-2θ) scans close to the $(\frac{3}{2},\frac{1}{2},4)$ Bragg position at several temperatures between 44.2 and 44.9 K for pure GdIn$_3$, while Fig. 9(a) displays the integrated intensity of both the central and satellite peaks, taken on warming and cooling. For $T < T_N^{bulk} = 44.15$ K, the central peak shows a smooth behavior. A fairly abrupt diminishment of the central peak intensity on warming is then observed at T_N^{bulk}, which coincides with the onset of the weak satellite peaks. The rise of these peaks is clearly insufficient to compensate the decrease of the central peak intensity, and therefore, the overall magnetic order parameter shows an abrupt change at T_N^{bulk}, consistent with the bulk paramagnetic first-order transition suggested by the specific heat results [see Fig. 1(a)]. The presence of thermal hysteresis seen in Fig. 9 is also characteristic of a first-order transition. Figure 10(a) shows the temperature dependence of the width of central and satellite
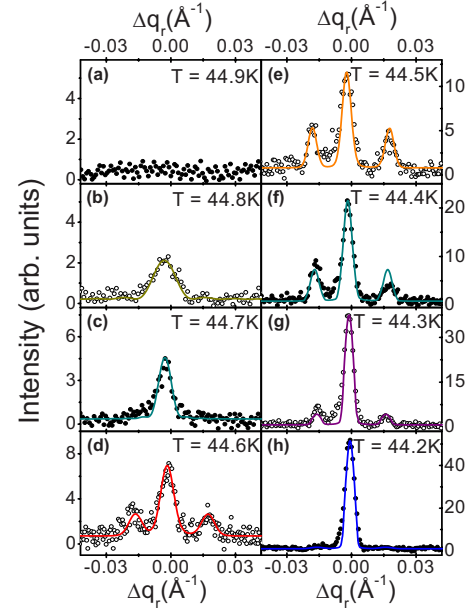

FIG. 8. (Color online) [(a)–(h)] Longitudinal scans around the $(\frac{3}{2},\frac{1}{2},4)$ reflection at selected T (symbols) and fits to the model depicted in Fig. 5(a) (lines).

peaks shown in Fig. 8 after deconvolution with the instrumental width. Above T_N^{bulk}, the central peak clearly broadens on warming, indicating that the EM-AFM near surface layer shows a temperature-dependent longitudinal correlation length. Figure 11(a) shows the EM-AFM layer thickness, obtained by fitting the observed intensities to the model described above (filled circles) in comparison to the correlation length for this phase, obtained from the $(\frac{3}{2},\frac{1}{2},4)$ peak width (open circles). Both quantities yield identical results, within the error bars, and decrease on warming. This indicates that the correlation length of the EM-AFM phase is limited by its thickness in the NSR. The width of the satellite peaks was also found to be temperature dependent. Indeed, a comparison between the AM-AFM layer thickness, obtained from the fits shown Figs. 5(a)–5(j) and 8(a)–8(h), and the correlation lengths obtained from the widths of the satellite peaks [Figs. 10(a)] also revealed that the correlation length of the AM-AFM phase is limited by its thickness. Above $T_N^{AM} = 44.65(5)$ K, the satellite peaks are not observed within our sensitivity. Finally, at $T_N^{NSR} = 44.85(5)$ K, the central peak suddenly disappears, signaling the near-surface paramagnetic transition. These results may be summarized in a depth-temperature phase diagram, displayed in Fig. 11(a).

5. (Ga,Cd)-substituted samples

The magnetic transition of the Ga- and Cd-substituted samples were also investigated in detail by magnetic x-ray diffraction. Figures 9(b) and 9(c) show the temperature dependence of the integrated intensity of the $(\frac{3}{2},\frac{1}{2},4)$ Bragg reflection of GdIn$_3$:Ga and GdIn$_3$:Cd, respectively. The associated peak widths, after deconvolution of the instrumental contribution, are indicated in Figs. 10(b) and 10(c). In addition to the slight changes in T_N (see Table I), interesting
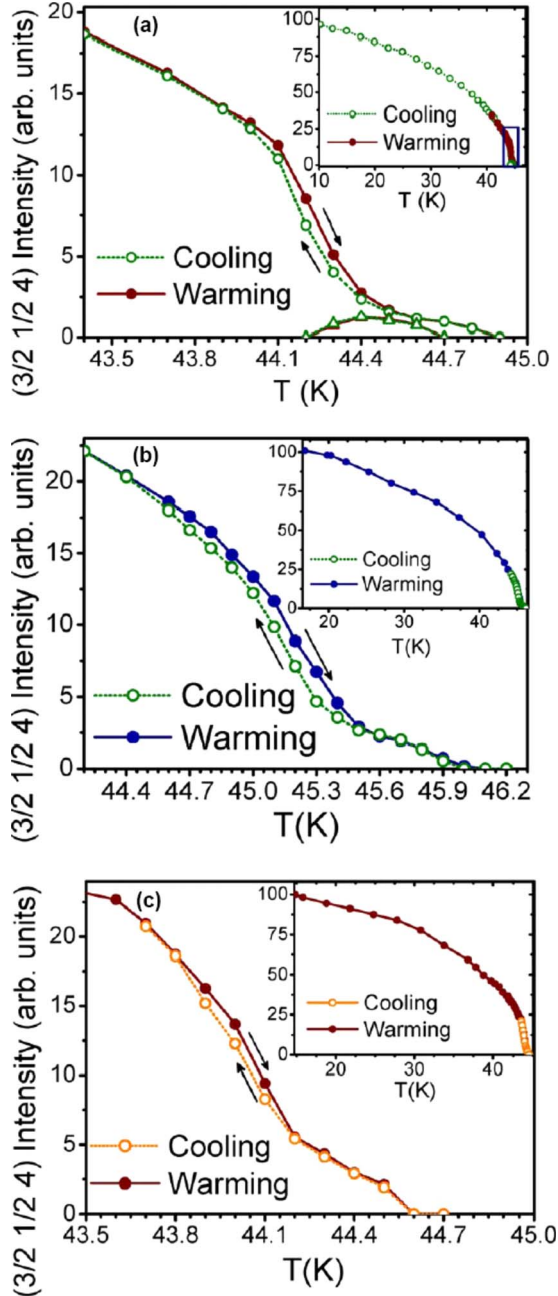
FIG. 9. (Color online) (a) Temperature dependence of the integrated intensities of the central (circles) and the sum of the satellite (triangles) magnetic peaks around the $(\frac{3}{2}, \frac{1}{2}, 4)$ reflection at the vicinity of T_N for (a) pure GdIn$_3$, (b) GdIn$_3$:Ga, and (c) GdIn$_3$:Cd. The inset shows the same in a more extended temperature range.

features were also seen. Particularly, two-step transitions were also observed, indicating distinct transition temperatures for the bulk and the NSR, with $T_N^{NSR} \sim T_N^{bulk} + 0.7$ K. Thermal hystereses have been observed close to T_N^{bulk} for both doped samples, indicating a first-order transition such as in the pure sample. However, satellite peaks were absent nearby the bulk transition, indicating that the AM-AFM phase evidenced for pure GdIn$_3$ is destroyed by the presence of small (~2%) substitution levels in the In site. The depth-temperature phase diagrams for the doped samples are given
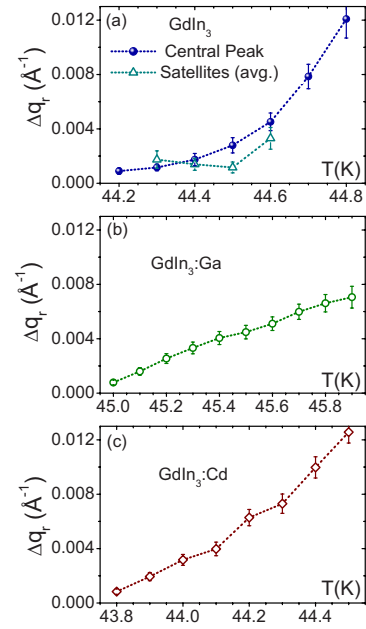

FIG. 10. (Color online) Temperature dependence of the widths of the central (circles) and the satellite (triangles) magnetic peaks around the $(\frac{3}{2}, \frac{1}{2}, 4)$ reflection at the vicinity of T_N for (a) GdIn$_3$, (b) GdIn$_3$:Ga, and (c) GdIn$_3$:Cd after deconvolution of the instrumental width.

in Figs. 11(b) and 11(c). It is important to note that these phase diagrams were constructed assuming that the EM-AFM layer thickness is identical to its correlation length. This hypothesis was experimentally verified only for the pure sample, in which the relative intensities of the central and satellite peaks for several (h, k, l) reflections allowed for an independent evaluation of the EM-AFM layer thickness. Rigorously, the experimental points in Figs. 11(b) and 11(c) are the correlation lengths across the $[\frac{3}{2}, \frac{1}{2}, 4]$ direction (which is nearly parallel to the surface normal $[0, 0, 1]$), and therefore, they may be considered as the lower limit of the EM-AFM layer thickness for the doped samples.

IV. DISCUSSION

We begin our discussion by the magnetic ground state. For all four pure and doped GdIn$_3$ samples studied in this work, a propagation vector $\vec{\tau} = [\frac{1}{2}, \frac{1}{2}, 0]$ was observed, where the $\vec{c}$ direction is the surface normal. Such a structure with FM chains along one cubic direction has been rationalized in terms of a competition among first- and second-neighbor Ruderman-Kittel-Kasuya-Yosida (RKKY) exchange interactions.[29] It is interesting to notice the absence of domains with $\vec{\tau} = [\frac{1}{2}, 0, \frac{1}{2}]$ and $\vec{\tau} = [0, \frac{1}{2}, \frac{1}{2}]$, which are symmetry equivalents to the observed $\vec{\tau}$ in a cubic structure. This rather surprising result may indicate a degeneracy removal caused by the surface so that the true ground state shows the ferromagnetic chains in Fig. 3 pointing along the surface normal. By considering the absence of any anisotropy in the Gd $4f^7$ orbitals, we associate this effect with the truncation of the long-range dipolar interactions at the surface. Of
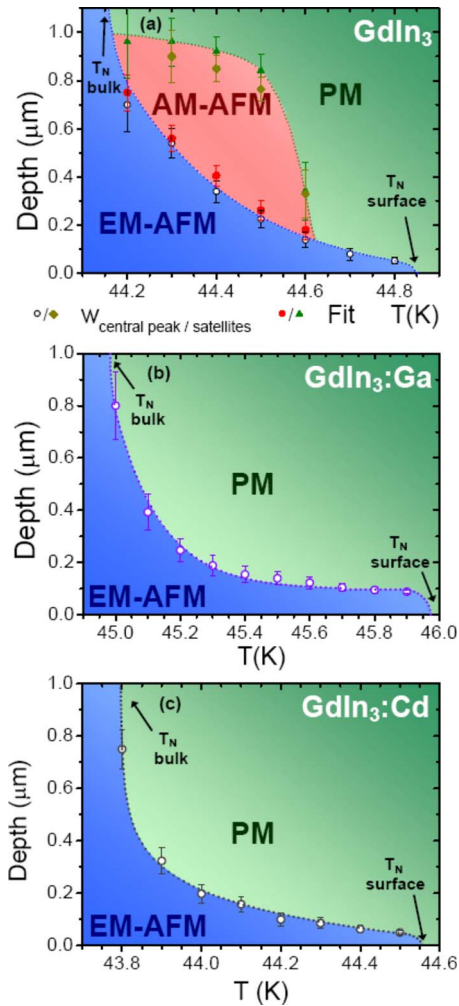
FIG. 11. (Color online) Depth-temperature magnetic phase diagram for (a) $GdIn_3$, (b) $GdIn_3:Ga$, and (b) $GdIn_3:Cd$, summarizing the results of this work. The results in (a) were independently obtained from the central and satellite peak widths shown in Fig. 10(a) (w) and from the fits shown in Figs. 8(a)–8(h).

course, this reasoning applies only for the near-surface region accessed by the x rays, and therefore, the other symmetry-equivalent AFM domains are expected to appear in bulk. Further experimental and theoretical investigations are needed to confirm or dismiss this hypothesis.

Undoubtedly, the most surprising results of this work arise at the vicinity of the magnetic transition temperature. We begin by summarizing the results shared by the pure and doped samples, in which the magnetic Bragg peaks corresponding to the commensurate structure with $\vec{\tau}=[\frac{1}{2},\frac{1}{2},0]$ show temperature intervals with distinct behaviors: (i) For $T \lesssim T_N^{bulk}$, the integrated intensities follow a conventional order parameter behavior, the peak widths are instrumental only, and no asymmetric shifts are observed. (ii) For $T \sim T_N^{bulk}$, a fairly abrupt decrease of the magnetic intensity is observed accompanied by thermal hysteresis. (iii) For $T_N^{bulk} < T \lesssim T_N^{NSR}$, the magnetic peaks broaden and show asymmetric shifts due to finite-sized correlation lengths (at this point, the integrated intensity remains in the level of $\sim 1\% - 2\%$ of

the maximum intensity at low temperatures for all studied samples). (iv) Finally, the reminiscent scattering suddenly disappears at $T_N^{NSR} \sim T_N^{bulk}+0.7$ K. While observations (i) and (ii) above are expected for first-order phase transitions, points (iii) and (iv) deserve a more careful account. The most straightforward explanation for the reminiscent scattering above T_N^{bulk} would be conventional critical scattering associated with dynamical short-range spin correlations. However, the relatively high intensities and sharp profiles for $T_N^{bulk} < T \lesssim T_N^{NSR}$, the abrupt disappearance of this signal above T_N^{NSR}, the coincidence of EM-AFM layer thickness, and correlation length [see Fig. 11(a)] are not consistent with this scenario, rather suggesting at least two distinct and well defined phase transitions, one for the bulk and the other for the NSR. We should mention that the relatively weak resonances at Gd L edges as compared to U M edges prevented us to obtain a detailed depth profile of the magnetism above T_N^{bulk} using magnetic truncation rod profiles such as in Refs. 10 and 16 for uranium compounds, and our instrumentation did not allow for a grazing-incidence geometry such as used in Ref. 15 for NiO. Still, our resonant diffraction results, complemented by bulk $C_p(T)$ and $\chi_{dc}(T)$ measurements, are sufficient to draw a rather interesting picture of the near-surface magnetism of $GdIn_3$ in the submicrometric scale.

The experimental facts described above allow us to associate the reminiscent magnetic scattering in pure and substituted $GdIn_3$ for $T_N^{bulk} < T \lesssim T_N^{NSR}$ to a near-surface-induced antiferromagnetism. This frozen magnetism at the near surface is presumably associated with a perturbation in the magnetic interactions, which may be caused either by the presence of the surface itself (causing a truncation of the exchange interactions) or by the lattice defects that are more likely to occur in the near-surface region of a polished surface. On the other hand, the typical thicknesses of the NSR found in this work ($\lesssim 1$ μm) are about 3 orders of magnitude larger than the typical range of the RKKY exchange interactions ($\lesssim 1$ nm). For this reason, it might appear implausible to associate the complex behavior found in the NSR to the surface itself. However, we argue that the proximity to a first-order transition may lead to an interface delocalization such as predicted theoretically for extraordinary transitions.[6] In fact, our results for both pure and doped $GdIn_3$ may be taken as an experimental evidence of interface delocalization in the submicrometric length scale.

While the Ga- and Cd-doped samples show a two-phase coexistence near T_N, the behavior of pure $GdIn_3$ is clearly richer, with a third, AM-AFM, phase sandwiched between the EM-AFM and PM phases. Since the PM phase do not contribute to the observable magnetic scattering, it is interesting to review the experimental evidence for this phase in the temperature interval in which contributions from the EM-AFM and AM-AFM phases were observed. Simulations of the scattering profiles of Figs. 5(a)–5(j) by a simpler model without the PM phase (i.e., with a bulk AM-AFM phase) overestimate the intensity of the satellite peaks of the reflections with the largest penetration depths, while the reflections with intermediate or smaller penetration depths remain well fitted (not shown). This is a clear indication of the finite depth of the AM-AFM phase. Also, the interesting temperature dependence of the width of the satellites [see Fig. 10(a)]

cannot be trivially understood with a two-phase model, being, however, entirely consistent with the three-phase picture drawn in Fig. 11(a). The hypothesis that the AM-AFM phase is not bulk representative is also indirectly supported by the $C_p(T)$ and $\chi_{dc}(T)$ measurements (see Fig. 1), which indicate a single bulk phase transition. In contrast, other RIn$_3$ (R = Nd, Sm) compounds show complex phase diagrams and successive phase transitions in narrow temperature intervals due to the competition of exchange interactions and spin anisotropies caused by $4f$ orbital moments and crystal field effects.[31] A prototypical example is NdIn$_3$, where three successive bulk magnetic transitions take place in a narrow temperature interval of about 1 K. In that case, a sine-modulated AM-AFM phase with $\vec{\tau} = (\frac{1}{2}, \frac{1}{2}, \delta)$ with $\delta = 0.037$ was observed between $T_N = 5.9$ K and 5.2 K. In addition, a second modulated phase with $\delta = 0.017$ takes place between 5.2 K and 4.7 K, and finally, an EM-AFM phase at (0.5 0.5 0) occurs below 4.7 K. All these bulk transitions were nicely captured by $\chi_{dc}(T)$ measurements.[31] Instead, our data for GdIn$_3$ show a single bulk transition, presumably between the low-temperature EM-AFM to the PM phase. We are therefore led to the conclusion that the AM-AFM phase observed by magnetic diffraction for the undoped samples is not bulk representative, but rather an intermediate phase sandwiched between the PM bulk and an EM-AFM phase in the NSR. Notice that the specific heat curves of pure and doped samples close to T_N^{bulk} are fairly similar [see Figs. 1(a)–1(c)], even though only the pure sample show the AM-AFM phase emerging between the EM-AFM and PM phases in our x-ray magnetic diffraction study. This gives additional support to the conclusion that the AM-AFM phase is not bulk representative.

The possible origin of the AM-AFM phase sandwiched between the EM-AFM near-surface region and the bulk PM phase is now discussed. As already mentioned, NdIn$_3$ and SmIn$_3$ show stable AM-AFM bulk phases at the vicinity of T_N due to a competition between exchange and anisotropy terms in the spin Hamiltonian. For Gd compounds with spherical $4f^7$ shell, anisotropy terms are arguably weaker, and a bulk AM-AFM phase does not appear to be stable at any temperature. Nonetheless, it is not unreasonable to assume that the free energies of the AM-AFM and EM-AFM phases are comparable for temperatures sufficiently close to T_N. Thus, in a scenario of a heterogeneous magnetic state associated with an extraordinary first-order transition, an intermediate AM-AFM state might develop between the EM-AFM and PM phases, possibly reducing the interface energy between these phases. In fact, the AM-AFM phase appears to arise in a delicately balanced physical state, which is easily destroyed by the small impurity levels induced by the Cd and Ga doping performed in this work.

Simultaneous occurrence of three phases in the near-surface region close to a first-order phase transition was theoretically predicted several years ago by Celestini and ten Bosch,[23] including the possibility of a macroscopic region with a metastable phase. Among the necessary conditions for the actual realization of this phenomenon are (i) the intermediary metastable state (AM-AFM, in our context) and the stable ordered state (EM-AFM) must be close in energy and (ii) the order parameter for the intermediary metastable and stable states must be close in value. Interestingly, both conditions appear to be satisfied in the present case. Condition (i) is evidenced by the presence of stable AM-AFM states in narrow temperature interval close to T_N in the related compounds NdIn$_3$ and SmIn$_3$ [see above], while condition (ii) was implicitly assumed in our fitting model [see Fig. 7(a)], which successfully accounted for magnetic scattering profiles around several Bragg positions. Therefore, our results may be taken as an experimental realization of the scenario predicted in Ref. 23. On the other hand, we believe that an additional ingredient accounting for the fact that $T_N^{NSR} > T_N^{bulk}$ in GdIn$_3$ (extraordinary transition) must be included in the scenario of Ref. 23 in order to account for the strongly temperature-dependent *static* three-phase coexistence observed here, as opposed to a *dynamical* coexistence occurring exactly at T_N in ordinary first-order transitions.

V. CONCLUSIONS

In summary, we observed complex depth-temperature phase diagrams in the submicrometric scale for (001) surfaces of pure and (Cd,Ga)-doped GdIn$_3$, which were ascribed to a delocalization of the interface between ordered and disordered states at the vicinity of a first-order phase transition. A third, amplitude-modulated AFM phase, connecting the equal-magnitude AFM near-surface region and the paramagnetic bulk, was observed and was shown to be very sensitive to dilute substitutions in the In site. These results were discussed in terms of a three-phase coexistence scenario theoretically proposed for first-order transitions.[23] The rich magnetic behavior in the near-surface region was observed in a length scale of $\sim 0.1-1$ μm toward the bulk, much larger than the $1-10$ nm scale observed in previous surface magnetic diffraction investigations in other compounds (see, for example, Refs. 15–17). This may be related to the fact that here the effects were observed at temperatures much closer to T_N^{bulk} (within an interval of ~ 1 K, i.e., $\delta T \sim 0.025 T_N$), pushing the interface(s) between the competing magnetic states deeper toward the bulk (see Ref. 18). Overall, our results reveal a surprisingly rich physics at the near-surface region of a model magnetic material, indicating that other compounds with first-order transitions and competitions among distinct ordered states may also present very interesting behaviors close to the surface. It is also clear from this work that magnetic intermetallics may be clean and experimentally accessible systems to test theoretical models for surface (spin) melting transitions.

*egranado@ifi.unicamp.br

[1] M. Pleimling, J. Phys. A **37**, R79 (2004).

[2] K. Binder, *Phase Transitions and Critical Phenomena* (Academic, London, 1983), Vol. 8, p. 1.

[3] A. B. Abraham, *Phase Transitions and Critical Phenomena* (Academic, London, 1986), Vol. 10, p. 1.

[4] H. W. Diehl, *Phase Transitions and Critical Phenomena* (Academic, London, 1986), Vol. 10, p. 75.

[5] R. Lipowsky, Phys. Rev. Lett. **49**, 1575 (1982); R. Lipowsky, D. M. Kroll, and R. K. P. Zia, Phys. Rev. B **27**, 4499 (1983).

[6] R. Lipowsky and W. Speth, Phys. Rev. B **28**, 3983 (1983).

[7] J. W. M. Frenken and J. F. van der Veen, Phys. Rev. Lett. **54**, 134 (1985).

[8] H. Dosch, L. Mailänder, H. Reichert, J. Peisl, and R. L. Johnson, Phys. Rev. B **43**, 13172 (1991).

[9] M. Altarelli, M. D. Nuñez-Regueiro, and M. Papoular, Phys. Rev. Lett. **74**, 3840 (1995).

[10] G. M. Watson, B. D. Gaulin, D. Gibbs, T. R. Thurston, P. J. Simpson, S. M. Shapiro, G. H. Lander, Hj. Matzke, S. Wang, and M. Dudley, Phys. Rev. B **53**, 686 (1996).

[11] S. Langridge, W. G. Stirling, G. H. Lander, J. Rebizant, J. C. Spirlet, D. Gibbs, and O. Vogt, Europhys. Lett. **25**, 137 (1994).

[12] K. Hirota, G. Shirane, P. M. Gehring, and C. F. Majkrzak, Phys. Rev. B **49**, 11967 (1994).

[13] T. R. Thurston, G. Helgesen, J. P. Hill, D. Gibbs, B. D. Gaulin, and P. J. Simpson, Phys. Rev. B **49**, 15730 (1994).

[14] P. M. Gehring, K. Hirota, C. F. Majkrzak, and G. Shirane, Phys. Rev. Lett. **71**, 1087 (1993).

[15] A. Barbier, C. Mocuta, W. Neubeck, M. Mulazzi, F. Yakhou, K. Chesnel, A. Sollier, C. Vettier, and F. de Bergevin, Phys. Rev. Lett. **93**, 257208 (2004).

[16] See, for example, A. Stunault, S. Langridge, C. Vettier, D. Gibbs, and N. Bernhoeft, Phys. Rev. B **55**, 423 (1997), and references therein.

[17] G. M. Watson, D. Gibbs, G. H. Lander, B. D. Gaulin, L. E. Berman, Hj. Matzke, and W. Ellis, Phys. Rev. Lett. **77**, 751 (1996); Phys. Rev. B **61**, 8966 (2000).

[18] B. Stahl, S. Bhattacharya, S. Gottschalk, J. Ellrich, H. Schmitt, J. Ebert, M. Ghafari, H. Hahn, A. Kamzin, D. Vcherashniy, and A. R. Raju, Phys. Rev. B **66**, 104426 (2002).

[19] C. Petrovic, R. Movshovich, M. Jaime, P. G. Pagliuso, M. F. Hundley, J. L. Sarrao, Z. Fisk, and J. D. Thompson, Europhys. Lett. **53**, 354 (2001).

[20] C. Petrovic, P. G. Pagliuso, M. F. Hundley, R. Movshovich, J. L. Sarrao, J. D. Thompson, Z. Fisk, and P. Monthoux, J. Phys.: Condens. Matter **13**, L337 (2001).

[21] P. G. Pagliuso, D. J. Garcia, E. Miranda, E. Granado, R. Lora-Serrano, C. Giles, J. G. S. Duque, R. R. Urbano, C. Rettori, J. D. Thompson, M. F. Hundley, and J. L. Sarrao, J. Appl. Phys. **99**, 08P703 (2006).

[22] R. Lora-Serrano, C. Giles, E. Granado, D. J. Garcia, E. Miranda, O. Agüero, L. Mendonça Ferreira, J. G. S. Duque, and P. G. Pagliuso, Phys. Rev. B **74**, 214404 (2006).

[23] F. Celestini and A. ten Bosch, Phys. Rev. E **50**, 1836 (1994).

[24] B. Vekemans, K. Janssens, L. Vincze, F. Adams, and P. Van Espen, X-Ray Spectrom. **23**, 278 (1994).

[25] F. He and P. J. Van Espen, Anal. Chem. **63**, 2237 (1991).

[26] M. O. Krause, J. Phys. Chem. Ref. Data **8**, 307 (1979).

[27] C. Giles, F. Yokaichiya, S. W. Kycia, L. C. Sampaio, D. C. Ardiles-Saravia, M. K. K. Franco, and R. T. Neuenschwander, J. Synchrotron Radiat. **10**, 430 (2003).

[28] I. K. Robinson, Phys. Rev. B **33**, 3830 (1986).

[29] E. Granado, B. Uchoa, A. Malachias, R. Lora-Serrano, P. G. Pagliuso, and H. Westfahl, Jr., Phys. Rev. B **74**, 214428 (2006).

[30] E. Granado, P. G. Pagliuso, C. Giles, R. Lora-Serrano, F. Yokaichiya, and J. L. Sarrao, Phys. Rev. B **69**, 144411 (2004).

[31] M. Amara, R. M. Galra, P. Morin, T. Veres, and P. Burlet, J. Magn. Magn. Mater. **130**, 127 (1994); M. Kasaya, B. Liu, M. Sera, T. Kasuya, D. Endoh, T. Goto, and T. Fujimura, *ibid.* **52**, 289 (1985); Z. Kletowski, Solid State Commun. **62**, 745 (1987).

[32] J. P. Hill and D. F. McMorrow, Acta Crystallogr., Sect. A: Found. Crystallogr. **52**, 236 (1996).

[33] S. W. Lovesey and S. P. Collings, *X-Ray Scattering and Absorption by Magnetic Materials* (Oxford Science, New York, 1996).

[34] N. Bernhoeft, G. H. Lander, M. J. Longfield, S. Langridge, D. Mannix, S. D. Brown, W. J. Nuttall, A. Hiess, C. Vettier, and P. Lejay, J. Phys.: Condens. Matter **16**, 3869 (2004).

[35] J. A. Blanco, D. Gignoux, and D. Schmitt, Phys. Rev. B **43**, 13145 (1991).

[36] M. Rotter, M. Loewenhaupt, M. Doerr, A. Lindbaum, and H. Michor, Phys. Rev. B **64**, 014402 (2001).

[37] J.-P. Ader and A. I. Buzdin, Phys. Lett. A **319**, 360 (2003).